

Enhanced production of direct photons in Au + Au collisions at $\sqrt{s_{NN}}=200$ GeV and implications for the initial temperature

- A. Adare,⁸ S. Afanasiev,²² C. Aidala,⁹ N.N. Ajitanand,⁴⁹ Y. Akiba,^{43,44} H. Al-Bataineh,³⁸ J. Alexander,⁴⁹
A. Al-Jamel,³⁸ K. Aoki,^{28,43} L. Aphecetche,⁵¹ R. Armendariz,³⁸ S.H. Aronson,³ J. Asai,⁴⁴ E.T. Atomssa,²⁹
R. Averbeck,⁵⁰ T.C. Awes,³⁹ B. Azmoun,³ V. Babintsev,¹⁸ G. Baksay,¹⁴ L. Baksay,¹⁴ A. Baldissari,¹¹ K.N. Barish,⁴
P.D. Barnes,³¹ B. Bassalleck,³⁷ S. Bathe,⁴ S. Batsouli,^{9,39} V. Baublis,⁴² F. Bauer,⁴ A. Bazilevsky,³ S. Belikov,^{3,21,*}
R. Bennett,⁵⁰ Y. Berdnikov,⁴⁶ A.A. Bickley,⁸ M.T. Bjorndal,⁹ J.G. Boissevain,³¹ H. Borel,¹¹ K. Boyle,⁵⁰
M.L. Brooks,³¹ D.S. Brown,³⁸ D. Bucher,³⁴ H. Buesching,³ V. Bumazhnov,¹⁸ G. Bunce,^{3,44} J.M. Burward-Hoy,³¹
S. Butsyk,^{31,50} S. Campbell,⁵⁰ J.-S. Chai,²³ B.S. Chang,⁵⁸ J.-L. Charvet,¹¹ S. Chernichenko,¹⁸ J. Chiba,²⁴
C.Y. Chi,⁹ M. Chiu,^{9,19} I.J. Choi,⁵⁸ T. Chujo,⁵⁵ P. Chung,⁴⁹ A. Churyn,¹⁸ V. Cianciolo,³⁹ C.R. Cleven,¹⁶
Y. Cobigo,¹¹ B.A. Cole,⁹ M.P. Comets,⁴⁰ P. Constantin,^{21,31} M. Csanad,¹³ T. Csorgo,²⁵ T. Dahms,⁵⁰ K. Das,¹⁵
G. David,³ M.B. Deaton,¹ K. Dehmelt,¹⁴ H. Delagrange,⁵¹ A. Denisov,¹⁸ D. d'Enterria,⁹ A. Deshpande,^{44,50}
E.J. Desmond,³ O. Dietzsch,⁴⁷ A. Dion,⁵⁰ M. Donadelli,⁴⁷ J.L. Drachenberg,¹ O. Drapier,²⁹ A. Drees,⁵⁰
A.K. Dubey,⁵⁷ A. Durum,¹⁸ V. Dzhordzhadze,^{4,52} Y.V. Efremenko,³⁹ J. Egdemir,⁵⁰ F. Ellinghaus,⁸
W.S. Emam,⁴ A. Enokizono,^{17,30} H. En'yo,^{43,44} B. Espagnon,⁴⁰ S. Esumi,⁵⁴ K.O. Eyser,⁴ D.E. Fields,^{37,44}
M. Finger,^{5,22} M. Finger, Jr.,^{5,22} F. Fleuret,²⁹ S.L. Fokin,²⁷ B. Forestier,³² Z. Fraenkel,^{57,*} J.E. Frantz,^{9,50}
A. Franz,³ A.D. Frawley,¹⁵ K. Fujiwara,⁴³ Y. Fukao,^{28,43} S.-Y. Fung,⁴ T. Fusayasu,³⁶ S. Gadrat,³²
I. Garishvili,⁵² F. Gastineau,⁵¹ M. Germain,⁵¹ A. Glenn,^{8,52} H. Gong,⁵⁰ M. Gonin,²⁹ J. Gosset,¹¹ Y. Goto,^{43,44}
R. Granier de Cassagnac,²⁹ N. Grau,²¹ S.V. Greene,⁵⁵ M. Grosse Perdekamp,^{19,44} T. Gunji,⁷ H.-Å. Gustafsson,³³
T. Hachiya,^{17,43} A. Hadj Henni,⁵¹ C. Haegemann,³⁷ J.S. Haggerty,³ M.N. Hagiwara,¹ H. Hamagaki,⁷ R. Han,⁴¹
H. Harada,¹⁷ E.P. Hartouni,³⁰ K. Haruna,¹⁷ M. Harvey,³ E. Haslum,³³ K. Hasuko,⁴³ R. Hayano,⁷ M. Heffner,³⁰
T.K. Hemmick,⁵⁰ T. Hester,⁴ J.M. Heuser,⁴³ X. He,¹⁶ H. Hiejima,¹⁹ J.C. Hill,²¹ R. Hobbs,³⁷ M. Hohlmann,¹⁴
M. Holmes,⁵⁵ W. Holzmann,⁴⁹ K. Homma,¹⁷ B. Hong,²⁶ T. Horaguchi,^{43,53} D. Hornback,⁵² M.G. Hur,²³
T. Ichihara,^{43,44} K. Imai,^{28,43} M. Inaba,⁵⁴ Y. Inoue,^{45,43} D. Isenhower,¹ L. Isenhower,¹ M. Ishihara,⁴³ T. Isobe,⁷
M. Issah,⁴⁹ A. Isupov,²² B.V. Jacak,^{50,†} J. Jia,⁹ J. Jin,⁹ O. Jinnouchi,⁴⁴ B.M. Johnson,³ K.S. Joo,³⁵ D. Jouan,⁴⁰
F. Kajihara,^{7,43} S. Kometani,^{7,56} N. Kamihara,^{43,53} J. Kamin,⁵⁰ M. Kaneta,⁴⁴ J.H. Kang,⁵⁸ H. Kanou,^{43,53}
T. Kawagishi,⁵⁴ D. Kawall,⁴⁴ A.V. Kazantsev,²⁷ S. Kelly,⁸ A. Khanzadeev,⁴² J. Kikuchi,⁵⁶ D.H. Kim,³⁵ D.J. Kim,⁵⁸
E. Kim,⁴⁸ Y.-S. Kim,²³ E. Kinney,⁸ A. Kiss,¹³ E. Kistenev,³ A. Kiyomichi,⁴³ J. Klay,³⁰ C. Klein-Boesing,³⁴
L. Kochenda,⁴² V. Kochetkov,¹⁸ B. Komkov,⁴² M. Konno,⁵⁴ D. Kotchetkov,⁴ A. Kozlov,⁵⁷ A. Kral,¹⁰ A. Kravitz,⁹
P.J. Kroon,³ J. Kubart,^{5,20} G.J. Kunde,³¹ N. Kurihara,⁷ K. Kurita,^{45,43} M.J. Kweon,²⁶ Y. Kwon,^{52,58} G.S. Kyle,³⁸
R. Lacey,⁴⁹ Y.-S. Lai,⁹ J.G. Lajoie,²¹ A. Lebedev,²¹ Y. Le Bornec,⁴⁰ S. Leckey,⁵⁰ D.M. Lee,³¹ M.K. Lee,⁵⁸ T. Lee,⁴⁸
M.J. Leitch,³¹ M.A.L. Leite,⁴⁷ B. Lenzi,⁴⁷ H. Lim,⁴⁸ T. Liška,¹⁰ A. Litvinenko,²² M.X. Liu,³¹ X. Li,⁶ X.H. Li,⁴
B. Love,⁵⁵ D. Lynch,³ C.F. Maguire,⁵⁵ Y.I. Makdisi,³ A. Malakhov,²² M.D. Malik,³⁷ V.I. Manko,²⁷ Y. Mao,^{41,43}
L. Maek,^{5,20} H. Masui,⁵⁴ F. Matathias,^{9,50} M.C. McCain,¹⁹ M. McCumber,⁵⁰ P.L. McGaughey,³¹ Y. Miake,⁵⁴
P. Mike,^{5,20} K. Miki,⁵⁴ T.E. Miller,⁵⁵ A. Milov,⁵⁰ S. Mioduszewski,³ G.C. Mishra,¹⁶ M. Mishra,² J.T. Mitchell,³
M. Mitrovska,⁴⁹ A. Morreale,⁴ D.P. Morrison,³ J.M. Moss,³¹ T.V. Moukhanova,²⁷ D. Mukhopadhyay,⁵⁵
J. Murata,^{45,43} S. Nagamiya,²⁴ Y. Nagata,⁵⁴ J.L. Nagle,⁸ M. Naglis,⁵⁷ I. Nakagawa,^{43,44} Y. Nakamiya,¹⁷
T. Nakamura,¹⁷ K. Nakano,^{43,53} J. Newby,³⁰ M. Nguyen,⁵⁰ B.E. Norman,³¹ A.S. Nyanin,²⁷ J. Nystrand,³³
E. O'Brien,³ S.X. Oda,⁷ C.A. Ogilvie,²¹ H. Ohnishi,⁴³ I.D. Ojha,⁵⁵ H. Okada,^{28,43} K. Okada,⁴⁴ M. Oka,⁵⁴
O.O. Omiwade,¹ A. Oskarsson,³³ I. Otterlund,³³ M. Ouchida,¹⁷ K. Ozawa,⁷ R. Pak,³ D. Pal,⁵⁵ A.P.T. Palounek,³¹
V. Pantuev,⁵⁰ V. Papavassiliou,³⁸ J. Park,⁴⁸ W.J. Park,²⁶ S.F. Pate,³⁸ H. Pei,²¹ J.-C. Peng,¹⁹ H. Pereira,¹¹
V. Peresedov,²² D.Yu. Peressounko,²⁷ C. Pinkenburg,³ R.P. Pisani,³ M.L. Purschke,³ A.K. Purwar,^{31,50}
H. Qu,¹⁶ J. Rak,^{21,37} A. Rakotozafindrabe,²⁹ I. Ravinovich,⁵⁷ K.F. Read,^{39,52} S. Rembeczki,¹⁴ M. Reuter,⁵⁰
K. Reygers,³⁴ V. Riabov,⁴² Y. Riabov,⁴² G. Roche,³² A. Romana,^{29,*} M. Rosati,²¹ S.S.E. Rosendahl,³³ P. Rosnet,³²
P. Rukoyatkin,²² V.L. Rykov,⁴³ S.S. Ryu,⁵⁸ B. Sahlmueller,³⁴ N. Saito,^{28,43,44} T. Sakaguchi,^{3,7,56} S. Sakai,⁵⁴
H. Sakata,¹⁷ V. Samsonov,⁴² H.D. Sato,^{28,43} S. Sato,^{3,24,54} S. Sawada,²⁴ J. Seele,⁸ R. Seidl,¹⁹ V. Semenov,¹⁸
R. Seto,⁴ D. Sharma,⁵⁷ T.K. Shea,³ I. Shein,¹⁸ A. Shevel,^{42,49} T.-A. Shibata,^{43,53} K. Shigaki,¹⁷ M. Shimomura,⁵⁴
T. Shohjoh,⁵⁴ K. Shoji,^{28,43} A. Sickles,⁵⁰ C.L. Silva,⁴⁷ D. Silvermyr,³⁹ C. Silvestre,¹¹ K.S. Sim,²⁶ C.P. Singh,²
V. Singh,² S. Skutnik,²¹ M. Sluneka,^{5,22} W.C. Smith,¹ A. Soldatov,¹⁸ R.A. Soltz,³⁰ W.E. Sondheim,³¹
S.P. Sorenson,⁵² I.V. Sourikova,³ F. Staley,¹¹ P.W. Stankus,³⁹ E. Stenlund,³³ M. Stepanov,³⁸ A. Ster,²⁵

S.P. Stoll,³ T. Sugitate,¹⁷ C. Suire,⁴⁰ J.P. Sullivan,³¹ J. Sziklai,²⁵ T. Tabaru,⁴⁴ S. Takagi,⁵⁴ E.M. Takagui,⁴⁷ A. Taketani,^{43,44} K.H. Tanaka,²⁴ Y. Tanaka,³⁶ K. Tanida,^{43,44} M.J. Tannenbaum,³ A. Taranenko,⁴⁹ P. Tarján,¹² T.L. Thomas,³⁷ M. Togawa,^{28,43} A. Toia,⁵⁰ J. Tojo,⁴³ L. Tomášek,²⁰ H. Torii,⁴³ R.S. Towell,¹ V-N. Tram,²⁹ I. Tserruya,⁵⁷ Y. Tsuchimoto,^{17,43} S.K. Tuli,² H. Tydesjö,³³ N. Tyurin,¹⁸ C. Vale,²¹ H. Valle,⁵⁵ H.W. van Hecke,³¹ J. Velkovska,⁵⁵ R. Vertesi,¹² A.A. Vinogradov,²⁷ M. Virius,¹⁰ V. Vrba,²⁰ E. Vznuzdaev,⁴² M. Wagner,^{28,43} D. Walker,⁵⁰ X.R. Wang,³⁸ Y. Watanabe,^{43,44} J. Wessels,³⁴ S.N. White,³ N. Willis,⁴⁰ D. Winter,⁹ C.L. Woody,³ M. Wysocki,⁸ W. Xie,^{4,44} Y.L. Yamaguchi,⁵⁶ A. Yanovich,¹⁸ Z. Yasin,⁴ J. Ying,¹⁶ S. Yokkaichi,^{43,44} G.R. Young,³⁹ I. Younus,³⁷ I.E. Yushmanov,²⁷ W.A. Zajc,⁹ O. Zaudtke,³⁴ C. Zhang,^{9,39} S. Zhou,⁶ J. Zimányi,^{25,*} and L. Zolin²²

(PHENIX Collaboration)

¹Abilene Christian University, Abilene, TX 79699, USA

²Department of Physics, Banaras Hindu University, Varanasi 221005, India

³Brookhaven National Laboratory, Upton, NY 11973-5000, USA

⁴University of California - Riverside, Riverside, CA 92521, USA

⁵Charles University, Ovocný trh 5, Praha 1, 116 36, Prague, Czech Republic

⁶China Institute of Atomic Energy (CIAE), Beijing, People's Republic of China

⁷Center for Nuclear Study, Graduate School of Science, University of Tokyo, 7-3-1 Hongo, Bunkyo, Tokyo 113-0033, Japan

⁸University of Colorado, Boulder, CO 80309, USA

⁹Columbia University, New York, NY 10027 and Nevis Laboratories, Irvington, NY 10533, USA

¹⁰Czech Technical University, Zikova 4, 166 36 Prague 6, Czech Republic

¹¹Dapnia, CEA Saclay, F-91191, Gif-sur-Yvette, France

¹²Debrecen University, H-4010 Debrecen, Egyetem tér 1, Hungary

¹³ELTE, Eötvös Loránd University, H - 1117 Budapest, Pázmány P. s. 1/A, Hungary

¹⁴Florida Institute of Technology, Melbourne, FL 32901, USA

¹⁵Florida State University, Tallahassee, FL 32306, USA

¹⁶Georgia State University, Atlanta, GA 30303, USA

¹⁷Hiroshima University, Kagamiyama, Higashi-Hiroshima 739-8526, Japan

¹⁸IHEP Protvino, State Research Center of Russian Federation, Institute for High Energy Physics, Protvino, 142281, Russia

¹⁹University of Illinois at Urbana-Champaign, Urbana, IL 61801, USA

²⁰Institute of Physics, Academy of Sciences of the Czech Republic, Na Slovance 2, 182 21 Prague 8, Czech Republic

²¹Iowa State University, Ames, IA 50011, USA

²²Joint Institute for Nuclear Research, 141980 Dubna, Moscow Region, Russia

²³KAERI, Cyclotron Application Laboratory, Seoul, Korea

²⁴KEK, High Energy Accelerator Research Organization, Tsukuba, Ibaraki 305-0801, Japan

²⁵KFKI Research Institute for Particle and Nuclear Physics of the Hungarian Academy of Sciences (MTA KFKI RMKI), H-1525 Budapest 114, POBox 49, Budapest, Hungary

²⁶Korea University, Seoul, 136-701, Korea

²⁷Russian Research Center "Kurchatov Institute", Moscow, Russia

²⁸Kyoto University, Kyoto 606-8502, Japan

²⁹Laboratoire Leprince-Ringuet, Ecole Polytechnique, CNRS-IN2P3, Route de Saclay, F-91128, Palaiseau, France

³⁰Lawrence Livermore National Laboratory, Livermore, CA 94550, USA

³¹Los Alamos National Laboratory, Los Alamos, NM 87545, USA

³²LPC, Université Blaise Pascal, CNRS-IN2P3, Clermont-Fd, 63177 Aubiere Cedex, France

³³Department of Physics, Lund University, Box 118, SE-221 00 Lund, Sweden

³⁴Institut für Kernphysik, University of Muenster, D-48149 Muenster, Germany

³⁵Myongji University, Yongin, Kyonggi-do 449-728, Korea

³⁶Nagasaki Institute of Applied Science, Nagasaki-shi, Nagasaki 851-0193, Japan

³⁷University of New Mexico, Albuquerque, NM 87131, USA

³⁸New Mexico State University, Las Cruces, NM 88003, USA

³⁹Oak Ridge National Laboratory, Oak Ridge, TN 37831, USA

⁴⁰IPN-Orsay, Université Paris Sud, CNRS-IN2P3, BP1, F-91406, Orsay, France

⁴¹Peking University, Beijing, People's Republic of China

⁴²PNPI, Petersburg Nuclear Physics Institute, Gatchina, Leningrad region, 188300, Russia

⁴³RIKEN, The Institute of Physical and Chemical Research, Wako, Saitama 351-0198, Japan

⁴⁴RIKEN BNL Research Center, Brookhaven National Laboratory, Upton, NY 11973-5000, USA

⁴⁵Physics Department, Rikkyo University, 3-34-1 Nishi-Ikebukuro, Toshima, Tokyo 171-8501, Japan

⁴⁶Saint Petersburg State Polytechnic University, St. Petersburg, Russia

⁴⁷Universidade de São Paulo, Instituto de Física, Caixa Postal 66318, São Paulo CEP05315-970, Brazil

⁴⁸System Electronics Laboratory, Seoul National University, Seoul, Korea

⁴⁹Chemistry Department, Stony Brook University, Stony Brook, SUNY, NY 11794-3400, USA

⁵⁰Department of Physics and Astronomy, Stony Brook University, SUNY, Stony Brook, NY 11794, USA

⁵¹SUBATECH (Ecole des Mines de Nantes, CNRS-IN2P3, Université de Nantes) BP 20722 - 44307, Nantes, France

⁵²*University of Tennessee, Knoxville, TN 37996, USA*

⁵³*Department of Physics, Tokyo Institute of Technology, Oh-okayama, Meguro, Tokyo 152-8551, Japan*

⁵⁴*Institute of Physics, University of Tsukuba, Tsukuba, Ibaraki 305, Japan*

⁵⁵*Vanderbilt University, Nashville, TN 37235, USA*

⁵⁶*Waseda University, Advanced Research Institute for Science and Engineering, 17 Kikui-cho, Shinjuku-ku, Tokyo 162-0044, Japan*

⁵⁷*Weizmann Institute, Rehovot 76100, Israel*

⁵⁸*Yonsei University, IPAP, Seoul 120-749, Korea*

(Dated: September 24, 2018)

The production of e^+e^- pairs for $m_{e^+e^-} < 0.3 \text{ GeV}/c^2$ and $1 < p_T < 5 \text{ GeV}/c$ is measured in $p + p$ and Au + Au collisions at $\sqrt{s_{NN}} = 200 \text{ GeV}$. Enhanced yield above hadronic sources is observed. Treating the excess as photon internal conversions, the invariant yield of direct photons is deduced. In central Au + Au collisions, the excess of direct photon yield over $p + p$ is exponential in transverse momentum, with inverse slope $T = 221 \pm 19^{\text{stat}} \pm 19^{\text{syst}} \text{ MeV}$. Hydrodynamical models with initial temperatures ranging from $T_{\text{init}} \sim 300\text{--}600 \text{ MeV}$ at times of $\sim 0.6\text{--}0.15 \text{ fm}/c$ after the collision are in qualitative agreement with the data. Lattice QCD predicts a phase transition to quark gluon plasma at $\sim 170 \text{ MeV}$.

PACS numbers: 13.85.Qk, 25.75.Cj, 12.38.Mh, 21.65.Qr

Experimental results from the Relativistic Heavy Ion Collider (RHIC) have established the formation of dense partonic matter in Au + Au collisions at $\sqrt{s_{NN}} = 200 \text{ GeV}$ [1]. The large energy loss of light quarks and gluons [2] as well as that of heavy quarks [3] indicates that the matter is very dense. The strong elliptic flow of light [4, 5] and charmed [3] hadrons indicates rapid thermalization. Such a hot, dense medium should emit thermal radiation [6]; the partonic phase is predicted to be the dominant source of direct photons with $1 < p_T < 3 \text{ GeV}/c$ in Au + Au collisions at RHIC [7].

Observation of thermal photons will allow determination of the initial temperature of the matter. However, the measurement of direct photons for $1 < p_T < 3 \text{ GeV}/c$ is notoriously difficult due to a large background from hadronic decay photons. Direct photons contribute only $\simeq 10\%$ above the background photon yield [7]. In general, any source of high energy photons can also emit virtual photons, which convert to low mass e^+e^- pairs. For example, gluon Compton scattering ($q + g \rightarrow q + \gamma$) has an associated process that produces low mass e^+e^- pairs through internal conversion ($q + g \rightarrow q + \gamma^* \rightarrow q + e^+e^-$). Consequently, we search for “quasi-real” virtual photons, which appear as low invariant mass e^+e^- pairs.

The relation between photon production and the associated e^+e^- pair production can be written as [8, 9]

$$\frac{d^2n_{ee}}{dm_{ee}} = \frac{2\alpha}{3\pi} \frac{1}{m_{ee}} \sqrt{1 - \frac{4m_e^2}{m_{ee}^2}} \left(1 + \frac{2m_e^2}{m_{ee}^2}\right) S d\eta \gamma \quad (1)$$

Here α is the fine structure constant, m_e and m_{ee} are the masses of the electron and the e^+e^- pair respectively, and S is a process dependent factor that goes to 1 as $m_{ee} \rightarrow 0$ or $m_{ee} \ll p_T$. Equation (1) also describes the relation between the photons from hadron decays (e.g. $\pi^0, \eta \rightarrow \gamma\gamma$, and $\omega \rightarrow \gamma\pi^0$) and the e^+e^- pairs from Dalitz decays ($\pi^0, \eta \rightarrow e^+e^-\gamma$ and $\omega \rightarrow e^+e^-\pi^0$). For π^0 and η , the

factor S is given by $S = |F(m_{ee}^2)|^2 (1 - \frac{m_{ee}^2}{M_h^2})^3$ [10], where M_h is the meson mass and $F(m_{ee}^2)$ is the form factor.

The factor S for a hadron h is zero for $m_{ee} > M_h$. We exploit this cut-off to separate the direct photon signal from the hadronic background. Since 80% of the hadronic photons are from π^0 decays, the signal to background (S/B) ratio for the direct photon signal improves by a factor of five for $m_{ee} > M_{\pi^0} = 135 \text{ MeV}/c^2$, thereby allowing a direct photon signal that is 10% of the background to be observed as a 50% excess of e^+e^- pairs.

In this Letter we present the analysis of e^+e^- pairs for $m_{ee} < 0.3 \text{ GeV}/c^2$ and for $1 < p_T < 5 \text{ GeV}/c$ in Au + Au and $p + p$ collisions at $\sqrt{s_{NN}} = 200 \text{ GeV}$ recorded during 2004 and 2005, respectively. The PHENIX detector [11] measures electrons in the two central arms, each covering $|\Delta\eta| \leq 0.35$ in pseudorapidity and $\pi/2$ in azimuthal angle. The Au + Au analysis [9, 12] uses 8×10^8 minimum bias (Min. Bias) events corresponding to $92.2^{+2.5\%}_{-3.0\%}$ of the inelastic Au + Au cross section. The beam-beam counters and zero degree calorimeters provide the Min. Bias trigger, as well as the centrality selection [13]. The $p + p$ analysis [14] uses 43 nb^{-1} of data recorded using the Min. Bias trigger and 2.25 pb^{-1} of single electron triggered data. Helium bags in both runs reduced the total conversion material, including the beam pipe, to $\sim 0.4\%$ of a radiation length.

All electrons and positrons with $p_T > 0.2 \text{ GeV}/c$ are combined into pairs. Pairs from photon conversions in the detector material are removed by a cut on the orientation of the pair in the magnetic field [9]. The combinatorial background is computed by mixing events and is subtracted [9, 12]. The S/B ratio is ~ 0.2 (at $m_{ee} = 0.3 \text{ GeV}$) to ~ 1.5 (at $m_{ee} = 0.1 \text{ GeV}/c^2$) for $p_T > 2 \text{ GeV}/c$ and 0.05 to 0.4 for $1 < p_T < 2 \text{ GeV}/c$. There are two sources of correlated background: two e^+e^- pairs from a meson decay and correlated hadrons decaying into two e^+e^- pairs, either within the same jet or in back-to-back jets.

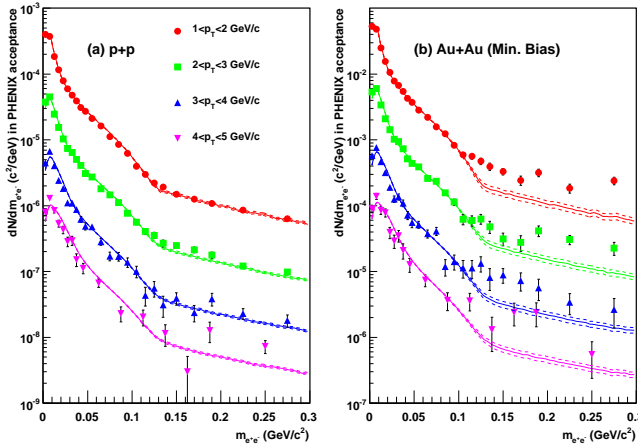


FIG. 1: (color online) The measured e^+e^- pair invariant mass distributions. The p_T ranges are shown in the legend. The solid curves represent an estimate of hadronic sources; the dashed curves represent the uncertainty in the estimate.

The magnitude of the correlated background, about 10% of the signal in $p + p$, is determined from the like-sign pair data and subtracted after correcting for acceptance differences between like and unlike-sign pairs [14]. We correct for electron reconstruction efficiency, and in $p + p$ for trigger efficiency, determined as a function of mass and pair p_T using a GEANT-based Monte Carlo simulation [15] of the PHENIX detector.

Figure 1 shows the mass spectra of e^+e^- pairs in $p + p$ and Au + Au collisions for different ranges of pair p_T , comparing to a “cocktail” of hadron decays calculated using a Monte Carlo hadron decay generator based on meson production measured by PHENIX [9]. Detector resolution is included in the cocktail calculation. The open charm contribution, calculated with PYTHIA [16], is also included but is negligible in this kinematic range. The cocktail is normalized to the data for $m_{ee} < 0.03 \text{ GeV}/c^2$; the absolute normalization agrees with the data within a 20% systematic uncertainty [12, 14]. The “knee” beginning at $m_{ee} \simeq 0.1 \text{ GeV}/c^2$ corresponds to the π^0 cut-off, leading to an 80% reduction of background above this point. The $p + p$ data are consistent with the background for $m_{ee} \geq M_{\pi^0}$ at lower p_T , but reveal a small excess over the background at higher p_T . A much greater excess is observed in Au + Au indicating enhanced production of virtual photons.

Internal conversion of direct photons is a possible source of the excess. Little contribution from other sources of e^+e^- pairs is expected in this mass region since $\pi^+\pi^- \rightarrow e^+e^-$ can only contribute for $m_{ee} \geq 2M_\pi$. Although PHENIX has observed a strong enhancement of e^+e^- pairs for $0.15 < m_{ee} < 0.75 \text{ GeV}/c^2$ in Au + Au, it peaks at low p_T and decreases rapidly with increasing

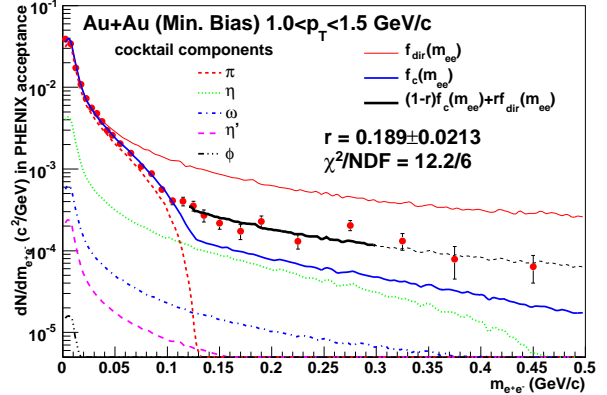


FIG. 2: (color online) Electron pair mass distribution for Au + Au (Min. Bias) events for $1.0 < p_T < 1.5 \text{ GeV}/c$. The two-component fit is explained in the text. The fit range is $0.12 < m_{ee} < 0.3 \text{ GeV}/c^2$. The dashed (black) curve at greater m_{ee} shows $f(m_{ee})$ outside of the fit range.

ing p_T [9] with a different mass distribution than that observed at high p_T .

Figure 2 shows that the mass spectrum for $m_{ee} < 0.5 \text{ GeV}/c^2$ and $p_T > 1 \text{ GeV}/c$ is well described by the cocktail plus internal conversion photons. The flat mass spectrum of the excess above the cocktail at this p_T shows no significant indication of low-mass enhancement [9]. Thus, we treat the excess entirely as internal conversion of photons and deduce the real direct photon yield from e^+e^- pairs using Eq. (1).

We fit a two-component function $f(m_{ee}) = (1 - r)f_c(m_{ee}) + r f_{\text{dir}}(m_{ee})$, to the mass distribution. $f_c(m_{ee})$ is the shape of the cocktail mass distribution (shown in Fig. 1), $f_{\text{dir}}(m_{ee})$ is the expected shape of the direct photon internal conversion, and r is the fit parameter. We assume that the form factor for direct photons is $F(m_{ee}^2) = 1$, as one would expect from a purely point-like process. For direct photons from parton fragmentation or from hadronic gas, $F(m_{ee}^2)$ may be greater than one. If we arbitrarily set the form factor in $f_{\text{dir}}(m_{ee})$ to be the same as that in $f_\eta(m_{ee})$, r would decrease by $\simeq 10\%$.

For each p_T bin, $f(m_{ee})$ is fit to the data for $m_{\text{low}} < m_{ee} < 0.3 \text{ GeV}/c^2$ with $m_{\text{low}} = 0.08, 0.1, 0.12 \text{ GeV}/c^2$; r is the only fit parameter. Figure 2 shows $f_{\text{dir}}(m_{ee})$ and $f_c(m_{ee})$ together with a fit result for Au + Au (Min. Bias) data for $1.0 < p_T < 1.5 \text{ GeV}/c$. For higher p_T bins, χ^2/NDF is near 1.0; fits to centrality separated data also give good χ^2/NDF .

Therefore, we focus on the uncertainties that can cause distortions in the mass distribution, namely (i) the particle composition in the hadronic background, (ii) the background (from mixed events and correlated pairs), (iii) the geometric acceptance due to detector active areas, and (iv) the efficiency corrections. These were studied by Monte Carlo simulation. The mass spectrum is

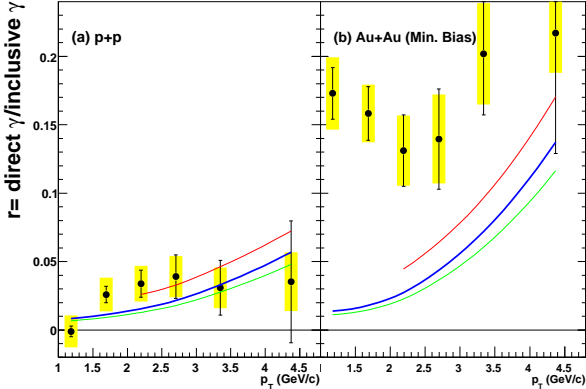


FIG. 3: (color online) The fraction of the direct photon component as a function of p_T . The error bars and the error band represent the statistical and systematic uncertainties, respectively. The curves are from a NLO pQCD calculation (see text).

distorted within the systematic uncertainties, and the fitting procedure is applied to the distorted spectrum to determine the systematic uncertainties in r . The systematic uncertainty due to the variation of m_{low} is also included. The dominant uncertainty is the particle composition in the hadronic cocktail, namely the η/π^0 ratio which is $0.48 \pm 0.03(0.08)$ at high p_T for $p + p$ ($\text{Au} + \text{Au}$) based on PHENIX measurements [17]. This corresponds to a $\simeq 7\%$ ($\simeq 17\%$) uncertainty in the $p + p$ ($\text{Au} + \text{Au}$) cocktail for $0.1 < m_{ee} < 0.3 \text{ GeV}/c^2$. Other sources cause only a few percent uncertainty in the data to cocktail ratio.

Figure 3 shows the fraction r of the direct photon component determined by the two-component fit in (a) $p + p$ and (b) $\text{Au} + \text{Au}$ (Min. Bias). The curves represent the expectations from a next-to-leading-order perturbative QCD (NLO pQCD) calculation [18]. For $p + p$, the curves show the ratio $d\sigma_\gamma^{NLO}(p_T)/d\sigma_\gamma^{\text{incl}}(p_T)$, where $d\sigma_\gamma^{NLO}(p_T)$ is the direct photon cross section from the NLO pQCD calculation and $d\sigma_\gamma^{\text{incl}}(p_T)$ is the inclusive photon cross section. For $\text{Au} + \text{Au}$, the curves represent $T_{\text{AA}} d\sigma_\gamma^{NLO}(p_T)/dN_\gamma^{\text{incl}}(p_T)$, where T_{AA} is the Glauber nuclear overlap function and $dN_\gamma^{\text{incl}}(p_T)$ is the inclusive photon yield. The three curves correspond, from top to bottom, to the theory scale $\mu = 0.5 p_T$, p_T , and $2 p_T$, respectively, showing the scale dependence of the theory. While the fraction r is consistent with the NLO pQCD calculation [18] in $p + p$, it is larger than the calculation in $\text{Au} + \text{Au}$ for $p_T < 3.5 \text{ GeV}/c$.

The direct photon fraction r in Fig. 3 is converted to the direct photon yield as $dN^{\text{dir}}(p_T) = r \times dN^{\text{incl}}(p_T)$. The inclusive photon yield $dN^{\text{incl}}(p_T)$ for each p_T bin is determined from the yield of e^+e^- pairs for $m_{ee} < 0.03 \text{ GeV}/c^2$ using Eq. (1). Here we use the fact that in

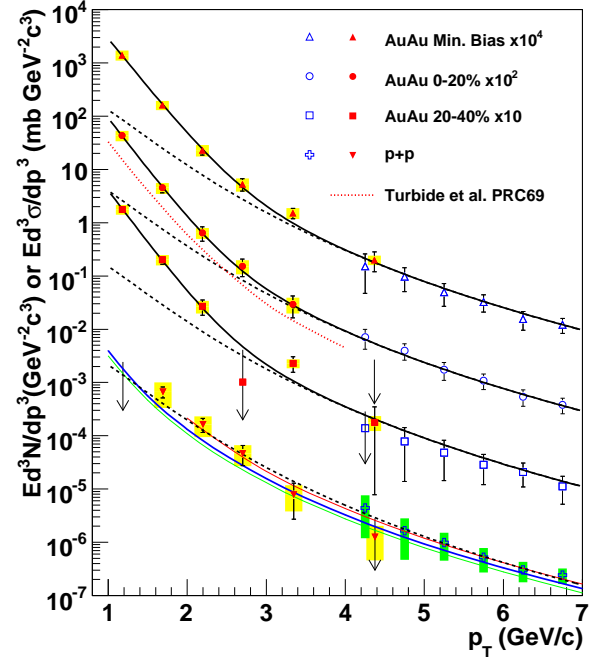


FIG. 4: (color online) Invariant cross section ($p + p$) and invariant yield ($\text{Au} + \text{Au}$) of direct photons as a function of p_T . The filled points are from this analysis and open points are from [19, 20]. The three curves on the $p + p$ data represent NLO pQCD calculations, and the dashed curves show a modified power-law fit to the $p + p$ data, scaled by T_{AA} . The dashed (black) curves are exponential plus the T_{AA} scaled $p + p$ fit. The dotted (red) curve near the 0-20% centrality data is a theory calculation [7].

this mass range the process dependent factor S is unity within a few percent for any photon source.

Figure 4 compares the direct photon spectra with previously measured direct photon data from [19, 20] and NLO pQCD calculations [18]. The systematic uncertainty of the inclusive photon (14% from the uncertainty in the e^+e^- pair acceptance correction[12]) is added in quadrature with the systematic uncertainties of these data. The $p + p$ data are shown as an invariant cross section using $d\sigma = \sigma_{pp}^{\text{inel}} dN$.

In this analysis we have converted the yield of excess e^+e^- pairs to that of real direct photons using Eq. (1), assuming $S = 1$. This implies $\frac{d^2n_{ee}}{dm_{ee}} = \frac{2\alpha}{3\pi} \frac{1}{m_{ee}} dn_\gamma$. Thus the yield of the excess e^+e^- pairs for $0.1 < m_{ee} < 0.3 \text{ GeV}/c^2$ before the conversion can be obtained by multiplying the direct photon yield by a factor of $\frac{2\alpha}{3\pi} \log \frac{300}{100} = 1.7 \times 10^{-3}$.

The pQCD calculation is consistent with the $p + p$ data within the theoretical uncertainties for $p_T > 2 \text{ GeV}/c$. A similarly good agreement is observed for π^0 [21]. The $p + p$ data can be well described by a modified power-law function ($A_{pp}(1+p_T^2/b)^{-n}$) as shown by the dashed curve in Fig. 4. The $\text{Au} + \text{Au}$ data are above the $p + p$ fit curve

scaled by T_{AA} for $p_T < 2.5$ GeV/ c , indicating that the direct photon yield in the low p_T range increases faster than the binary NN collision scaled $p + p$ cross section.

TABLE I: Summary of the fits. The first and second errors are statistical and systematic, respectively.

centrality	$dN/dy(p_T > 1\text{GeV}/c)$	$T(\text{MeV})$	χ^2/DOF
0-20%	$1.50 \pm 0.23 \pm 0.35$	$221 \pm 19 \pm 19$	4.7/4
20-40%	$0.65 \pm 0.08 \pm 0.15$	$217 \pm 18 \pm 16$	5.0/3
Min. Bias	$0.49 \pm 0.05 \pm 0.11$	$233 \pm 14 \pm 19$	3.2/4

We fit an exponential plus the T_{AA} -scaled $p + p$ fit function ($Ae^{-p_T/T} + T_{AA} \times A_{pp}(1 + p_T^2/b)^{-n}$) to the Au + Au data. The only free parameters in the fit are A and the inverse slope T of the exponential term. The systematic uncertainties in T are estimated by changing the $p + p$ fit component and the Au + Au data points within the systematic uncertainties. The results of the fits are summarized in Table I, where A is converted to dN/dy for $p_T > 1\text{GeV}/c$. For central collisions $T = 221 \pm 19^{\text{stat}} \pm 19^{\text{syst}}$ MeV. Using, instead, a power-law function ($\propto p_T^{-n}$) to fit the $p + p$ spectrum yields $n = 5.40 \pm 0.15$, and $T_{\text{AuAu}} = 240 \pm 21$ MeV. If the direct photons in Au + Au collisions are of thermal origin, the inverse slope T is related to the initial temperature T_{init} of the dense matter. In hydrodynamical models, T_{init} is 1.5 to 3 times T due to the space-time evolution [22]. Several hydrodynamical models can reproduce the central Au + Au data within a factor of two [9]. These assume formation of a hot system with initial temperature ranging from $T_{\text{init}} = 300$ MeV at thermalization time $\tau_0 = 0.6$ fm/ c to $T_{\text{init}} = 600$ MeV at $\tau_0 = 0.15$ fm/ c [22]. As an example, the dotted (red) curve in Fig. 4 shows a thermal photon spectrum in central Au + Au collisions calculated with $T_{\text{init}} = 370$ MeV [7].

In conclusion, we have measured e^+e^- pairs with $m_{ee} < 300$ MeV/ c^2 and $1 < p_T < 5$ GeV/ c in $p + p$ and Au + Au collisions. The $p + p$ data show a small excess over the hadronic background while the Au + Au data show a much larger excess. By treating the excess as internal conversion of direct photons, the direct photon yield is deduced. The yield is consistent with a NLO pQCD calculation in $p + p$. In central Au + Au collisions the shape of the direct photon spectrum above the

T_{AA} -scaled $p + p$ spectrum is exponential in p_T , with an inverse slope $T = 221 \pm 19^{\text{stat}} \pm 19^{\text{syst}}$ MeV. Hydrodynamical models with $T_{\text{init}} \sim 300$ –600 MeV at $\tau_0 \sim 0.6$ –0.15 fm/ c are in qualitative agreement with the data. Lattice QCD predicts a phase transition from hadronic phase to quark gluon plasma at ~ 170 MeV[1].

We thank the staff of the Collider-Accelerator and Physics Departments at BNL for their vital contributions. We acknowledge support from the Department of Energy and NSF (USA), MEXT and JSPS (Japan), CNPq and FAPESP (Brazil), NSFC (China), MSMT (Czech Republic), IN2P3/CNRS, and CEA (France), BMBF, DAAD, and AvH (Germany), OTKA (Hungary), DAE (India), ISF (Israel), NRF (Korea), MES, RAS, and FFAE (Russia), VR and KAW (Sweden), U.S. CRDF for the FSU, US-Hungarian NSF-OTKA-MTA, and US-Israel BSF.

* Deceased

† PHENIX Spokesperson: jacak@skipper.physics.sunysb.edu

[1] K. Adcox et al., Nucl. Phys. A **757**, 184 (2005).
[2] K. Adcox et al., Phys. Rev. Lett. **88**, 022301 (2002).
[3] A. Adare et al., Phys. Rev. Lett. **98**, 172301 (2007).
[4] K. H. Ackermann et al., Phys. Rev. Lett. **86**, 402 (2001).
[5] S. S. Adler et al., Phys. Rev. Lett. **91**, 182301 (2003).
[6] P. Stankus, Ann. Rev. Nucl. Part. Sci. **55**, 517 (2005).
[7] S. Turbide, R. Rapp, and C. Gale, Phys. Rev. **C69**, 014903 (2004).
[8] P. Lichard, Phys. Rev. **D51**, 6017 (1995).
[9] A. Adare et al., arXiv:0911.0244 [nucl-ex].
[10] L. G. Landsberg, Phys. Rept. **128**, 301 (1985).
[11] K. Adcox et al., Nucl. Instrum. Meth. **A499**, 469 (2003).
[12] S. Afanasiev et al. arXiv:0706.3034 [nucl-ex].
[13] S. S. Adler et al., Phys. Rev. **C69**, 034909 (2004).
[14] A. Adare et al., Phys. Lett. **B670**, 313 (2009).
[15] GEANT3.21 CERN Program Library.
[16] T. Sjöstrand et al., Comp. Phys. Comm. **135**, 238 (2001).
[17] S. S. Adler et al., Phys. Rev. Lett. **96**, 202301 (2006).
[18] L. E. Gordon and W. Vogelsang, Phys. Rev. **D48**, 3136 (1993); W. Vogelsang calculated the cross section.
[19] S. S. Adler et al., Phys. Rev. Lett. **94**, 232301 (2005).
[20] S. S. Adler et al., Phys. Rev. Lett. **98**, 012002 (2007).
[21] S. S. Adler et al., Phys. Rev. Lett. **91**, 241803 (2003).
[22] D. d'Enterria and D. Peressounko, Eur. Phys. J. **C46**, 451 (2006) and references therein.